Sulfate performance of blended cements (limestone and illite calcined clay) exposed to aggressive environment after casting

Agustín Rossetti[1], Tai Ikumi[2,3], Ignacio Segura[2,3], Edgardo F. Irassar[4,*]

[1] Comisión de Investigaciones Científicas de la Provincia de Buenos Aires, CICPBA- LEMIT, La Plata, Argentina. email: agustin.rossetti@ing.unlp.edu.ar

[2] Smart Engineering, Jordi Girona 1-3 K2M 202c, Barcelona, Spain – ORCID 0000-0001-9547-5241

[3] Department of Civil and Environmental Engineering, Universitat Politècnica de Catalunya Barcelona Tech, Jordi Girona 1-3, C1, E-08034 Barcelona, Spain. ORCID 0000-0001-6519-9899

[4] Facultad de Ingeniería, CIFICEN (UNCPBA-CICPBA-CONICET), B7400JWI Olavarría, Argentina. firassar@fio.unicen.edu.ar; ORCID 0000-0003-4488-0014

*Corresponding author

ABSTRACT

This paper evaluates how early aggressive exposure affects the sulfate resistance of blended cements containing limestone filler and/or calcined clay. Mortar and cement paste specimens were elaborated with different combinations of limestone filler and two different illitic calcined clays and exposed to a sodium sulfate solution shortly after casting. Assessment of sulfate resistance was based on expansion, mass variation, and compressive strength. Microscale evolution and distribution were examined by mercury intrusion porosimetry, X-ray diffraction, and scanning electron microscopy with energy-dispersive spectrometry measurements. Results prove superior sulfate resistance of compositions with high calcined clay content over limestone filler addition. Furthermore, the results reported suggest that the pozzolanic reaction progresses enough to reduce the sulfate ingress even at early exposure conditions. Therefore, calcined clay replacement can still provide effective pore refinement to limit sulfate penetration, increase strength, and reduce available CH to limit expansive phase formation.

Keywords: Illite calcined clay, limestone filler, sulfate attack, curing, early exposure.

1. INTRODUCTION

Calcined clays are arising as effective supplementary cementitious materials (SCMs) for blended cements due to several reasons: high availability, shortage of fly ash and slag, relative low activation temperature, low CO_2 emissions, and low uptake by other industries [1–4]. Additionally, Its incorporation in the concrete mixture improves the microstructure and refines the pore structure of cement paste [5]. Calcined clays may be high or low reactive pozzolan depending on the main clay mineral activated [6,7].

Low-grade kaolinitic calcined clay has been extensively investigated for use as SCM [8–10], especially combined with limestone filler, called LC^3 cements [11–14]. The concrete performance of these cements has been studied from a mechanical [15] and durable [16] point of view.

Illite is an abundant clay mineral around the world [17], which develops pozzolanic properties when thermally activated at 950 °C [16–20] due to the formation of amorphous aluminosilicate after its de-hydroxylation and structural collapse [22]. Illitic calcined clay (ICC) has been less investigated, and some authors consider that ICCs have a low reactivity [20] while others report good performance after 28 days [23]. Concrete performance with blended cements containing different calcined pozzolans has been compared recently [24,25]. Also, the combination of ICC and limestone filler (LF) was recently studied [26].

The complementary effect of LF and SCM has been widely reported [27,28]. LF stimulates the Portland cement hydration at early age when the particles are moistened by the mixing water [29]. However, when the replacement increases, the dilution effect cannot be compensated, resulting in reduced performance of the blend [30]. Moreover, shortly after casting, the contribution due to the pozzolanic activity of calcined clays is low, except for those containing metakaolinite (MK). At later ages, the stimulation on the hydration of portland cement loses importance, and the dilution effect must be compensated by the reaction of calcined clays producing C-(A)-S-H and AFm phases that reduce the porosity. The interaction between LF and calcined clays promotes the formation of monocarboaluminates, which may have a positive effect on sulfate resistance by stabilizing ettringite [31].

The sustainability of the construction industry also depends on the improvement of durability of real concrete structures, which are commonly exposed to a wide variety of aggressive conditions. According to Aïtcin & Mindess [32], to make a durable structure it is necessary the use of appropriate cements and aggregates which can proportionate a concrete having low w/b (< 0.40) that keeps its fluidity for about 90 minutes, placing it correctly and curing it appropriately with water. In terms of durability, the external sulfate attack (ESA) is a complex degradation phenomenon that may compromise the long-term durability of concrete exposed to sulfate-rich environments [33]. Sulfate ions penetrate into the concrete reacting with CH to form gypsum

($C\underline{S}H_2$) and with the AFm phases (C_4AH_{13} ; $C_4A\underline{S}H_{12-18}$; $C_4A\underline{C}H_{11}$) to form ettringite ($C_6A\underline{S}_3H_{32}$) [32-33]. The formation of these phases can generate expansive forces at the pore level leading to expansion and cracking [32-33]. In the presence of carbonate ions, abundant moisture, and low temperature, thaumasite ($C_3S\underline{S}\underline{C}H_{15}$) can form from the decomposition of the C-S-H, resulting in strength loss of concrete [36–38].

Several authors have studied the sulfate resistance of cement blends with calcined clays. Wild et al. [39] reported that 10 and 20 % replacement of MK prevents sulfate attack due to the CH consumption and pore structure refinement. Trümer & Ludwig [40] studied the sulfate performance of different types of calcined clays (illite, montmorillonite, and kaolinite with a 30% by mass replacement) on German mortar flat prisms exposed to 0.44 % Na_2SO_4 solution at 5 and 20 °C during six months. At 20 °C, CEM I and the blended cements with illite and montmorillonite exceeded the limit of 0.10 % expansion approximately at the same age. However, in the long term, the blended cements showed an increased sulfate resistance compared to the reference CEM I samples. Cordoba et al. [41,42] reported that the performance of illitic calcined clays depends on the replacement level and the C_3A content of the Portland cement used. A recent study presented by Shi et al. [43] assessed the sulfate resistance of calcined clay (CC) – LF – Portland cements exposed to a 0.11 M Na_2SO_4 solution at 5 and 20 °C. The authors showed that mortars containing MK or calcined montmorillonite and LF (35 %w/w replacement) of a white Portland cement or an ordinary Portland clinker with $CC/(CC+LF) \geq 0.5$ exhibited excellent sulfate resistance. The CH-consumption by the pozzolanic reactions of calcined clays and the dilution of the Portland clinker lead to a lower amount of calcium available for the secondary formation of gypsum and ettringite, which is identified as the main reason for the excellent sulfate resistance of the ternary cement blend [44,45].

Amongst the studies previously described, all exposed the specimens to the sulfate solution after a period of non-aggressive curing ranging from 12 – 91 days. However, sulfate ions are usually found in sulfate-rich soils and underground waters in contact with concrete. Therefore, ESA is especially significant in underground structures like foundations, dams, tunnels, or waste containers. Due to the large size and monolithic requirements, these structures are usually cast *in situ* and are thus subjected to sulfates shortly after casting. Nevertheless, most current laboratory studies about ESA are performed on specimens cured several days in lime water before immersion in the aggressive sulfate solution [46]. This non-aggressive curing may be extended, especially for blended cements with a high volume of SCM, up to 90 days, which is far from realistic field exposure ages. When cementitious materials are immersed in a sulfate solution, there is a competition between the cement hydration reactions that determines the microstructure and the kinetics of sulfate attack, being its effects scarcely studied.

Al-Akhras [47] studied the sulfate performance of concretes made with different percentages of MK-replacement cured 3, 7, and 28 days in lime-water before being exposed to a high-concentration sulfate

solution. After 18 months, all MK concrete specimens obtained similar resistance to sulfate attack, and the author concluded insignificant effects of the curing period adopted. However, the use of MK in mass concrete is limited by its high cost, high water demand, and high reactivity, which causes the release of high hydration heat. No studies were found investigating these effects on ICC cement blends, more appropriate for the mass concrete applications most likely exposed to ESA.

The aim of this study is the comparison of the sulfate performance of blended cements containing LF and/or ICC without previous non-aggressive curing. For this purpose, the interactions between the hydration reactions and the sulfate attack were studied in cement paste cubes by visual inspection, mass measurements, and evaluation of the mineralogical composition at the surface and the core of specimens. Additionally, MIP studies were carried out to characterize the pore network. The expansion, mass variation, and compressive strength were evaluated on standard mortar samples. Penetration profiles and scatter plots were obtained after one year of sulfate exposure by energy-dispersive spectrometry measurements to determine the distribution and composition of the microstructure.

2. MATERIALS AND TEST METHODS

2.1. Materials

Portland cement (CEM I 52.5R) with 12.3 % C_3A content, limestone filler composed by high purity calcite (LF), and two different illitic calcined clays (identified by their color: Red (ICCR) and Orange (ICCO)) were selected to produce the pastes and mortars used in this study. The illitic clay-stones from quarries near Olavarría, Buenos Aires Province (Argentine), were calcined in an oven at 950 °C and grounded in a laboratory ball mill until 90 % of particles were less than 45 μm. The calcination temperature was selected according to the results of previous studies [48,49]. Both calcined clays meet the chemical requirements for Class N pozzolan (ASTM C618). XRD analysis reveals low-intensity peaks of dehydroxylated illite in both clays, and the associated minerals are quartz and hematite for ICCR and quartz, hematite, feldspar, and hercynite for ICCO. For both illitic calcined clays, the Frattini test was positive after 14 days [19,47]

Table 1 summarizes the phase and chemical compositions of the binders determined by quantitative XRD and XRF spectrometry, respectively. The mineralogical composition of the cement was estimated by Bogue equations. Data provided by Bogue equations is only used qualitatively to classify the cement.

Table 1. Phase and chemical composition of binders

Chemical composition, %	CEM I 52.5R	LF	ICCR	ICCO
CaO	60.92	59.53	0.33	1.13
SiO_2	19.50	<0.01	66.30	63.43
Al_2O_3	5.90	1.10	16.28	13.82
Fe_2O_3	1.70	0.52	9.23	7.89
MgO	2.10	0.48	1.46	2.71
SO_3	3.50	0.06	<0.01	0.04
K_2O	0.78	0.06	5.60	4.29
Na_2O	0.35	<0.01	0.08	1.52
LOI	3.00	39.98	0.58	0.20
Mineralogical composition, %				
C_3S	65.4	-	-	-
C_2S	10.6	-	-	-
C_3A	12.3	-	-	-
C_4AF	5.6	-	-	-
Gypsum	5.8	-	-	-
Calcite	-	98.5	-	-
Quartz	-	-	35.0	31.0
Feldspar	-	-	-	17.0
Hematite	-	-	5.0	2.0
Hercynite,	-	-	-	1.0
Anhydrous illite	-	-	4.0	3.0
Amorphous phase	-	-	56.0	46.0

The physical characteristics of the materials are summarized in Table 2. Density was determined by the procedure described in ASTM C 188. The Blaine method (ASTM C 204) and the BET technique (ISO 9277) were used to characterize the specific surface area. The particle size distribution (PSD) was determined using the laser granulometer (Malvern Mastersizer 2000), and the PSD curve can be found elsewhere [50]. Table 2 includes the compressive strength index (CSI) at 7, 28, and 90 days for the two illitic clays. These were obtained as the ratio of the mortar compressive strength of blended cement with 25% replacement by mass at constant w/cm (0.50) and the compressive strength of normalized OPC control mortar. According to the BS 8615-1 (BS 8615-1, 2019), the CSI of SCM pozzolans should be greater than 0.75 and 0.85 at 28 and 90 days, respectively.

Table 2. Physical properties of the binders

Physical properties	CEM I 52.5R	LF	ICCR	ICCO
Density, g/cm^3	3.10	2.70	2.63	2.65
Particle size distribution, μm				
Dv10	0.58	1.7	1.6	1.3
Dv50	6.88	6.6	8.8	7.3
Dv90	31.84	72.2	33.7	36.9
Specific surface area				
BET, m^2/g	1.1	3.74	1.6	
Blaine, m^2/kg	496	717	522	724
Compressive strength index				
7 days	-	-	0.85	0.76
28 days	-	-	0.96	0.86
90 days	-	-	1.05	0.97

2.2. Composition and preparation of paste and mortar specimens

Five blended cements with different combinations of ICCO and ICCR replacement (0, 15, and 30 % by cement mass) were prepared to assess the performance of these illitic calcined clays in a sulfate-rich environment. LF was introduced in the mixtures with 0 and 15 % ICC replacement to maintain constant the cement content amongst all compositions tested (SCM replacement in all binders was set to 30% by cement weight). In this way, all compositions present the same initial C_3A content, and thus, the different performance observed can be mainly attributed to the effects of the SCMs introduced. Table 3 presents the different blended cements and the nomenclature adopted in each case.

Table 3. Composition of blended cements adopted, in wt-%

	C30F	C30R	C30O	C15F15R	C15F15O
CEM I 52.5R	70	70	70	70	70
LF	30	-	-	15	15
ICCR	-	30	-	15	-
ICCO	-	-	30	-	15

Paste cubes of 20 x 20 x 20 mm, mortar cubes of 25 x 25 x 25 mm, and mortar prisms of 25 x 25 x 297 mm for micro and macrostructural characterization were cast using the blended cements listed in Table 3. Both pastes and mortars adopted a water to binder ratio of 0.485, as prescribed by ASTM C1012. Mortars have a cement to graded-sand ratio of 1:2.75, and a standard mixing procedure was adopted. All SCMs used were thoroughly homogenized with Portland cement before water addition.

Paste and mortar specimens were cured in a moist cabinet at 20 ± 1°C for 24 h. Then, specimens were demolded and immersed in lime water at 20 ± 1 °C for 24 hours to ensure complete saturation of the samples before sulfate exposure. Finally, two days after casting, specimens were immersed in the standard exposure solution described in the ASTM C1012 (50 g/l Na_2SO_4). Reference samples of each composition were exposed to non-aggressive curing with water without sulfates for comparative purposes. The solutions were renewed every week during the first month and monthly until the end of all tests. The early sulfate exposure adopted in this study intends to reproduce the realistic conditions of structures built *in situ*, exposed to the sulfate-rich environment since casting, and accelerating the attack.

2.3. Test methods

185 Table 4 describes the tests performed on the paste cubes (20x20x20 mm), mortar cubes (25x25x25 mm), and
186 mortar prisms (25x25x297 mm), which cover a wide range of techniques for assessing the macro and
187 microstructural behavior of the mixtures during the ESA.
188
189 Table 4. Tests performed on paste and mortar specimens

Test	Specimen		Nº Replicas	Time (days)
Visual inspection	Paste	20x20x20 mm	6	28/96/204
	Mortar	25x25x25 mm	4	7/28/90/180/365
Mass change	Paste	20x20x20 mm	12	7/14/28/56/96/204
	Mortar	25x25x297 mm	4	7/14/21/28/56/91/105/120/180/365
Compressive strength	Mortar	25x25x25 mm	4	7/28/90/180/365
Expansion	Mortar	25x25x297 mm	6	7/14/21/28/56/91/105/120/180/365/ 540/720
MIP	Paste	5 mm by 10 mm diameter	2	28
XRD	Paste	20x20x20 mm surface and core	1	28/204
	Mortar	25x25x297 mm bulk	1	365
SEM	Mortar	25x25x297 mm cross section	1	365

190
191 Macroscale behavior was characterized by expansion, mass, compressive strength, and visual aspect.
192 Specimens were visually inspected to identify cracking, change of color, or any other sign of deterioration.
193 Mass evolution was controlled with a precision balance of ± 0.01 g after drying the surface water of the
194 samples. Length change was measured following the procedure defined by the ASTM C 1012. Compressive
195 strength tests were performed on mortar cubes according to ASTM C 109.
196
197 Microscale evolution during the ESA is examined by mercury intrusion porosimetry (MIP), X-ray diffraction
198 (XRD), and scanning electron microscopy (SEM). Pore size distribution of the pastes was measured with a
199 Pascal 140 and Pascal 440 porosimeters (Thermo Scientific) measuring the 4–100 μm and the 7–4000 nm pore
200 radium. Paste (w/cm = 0,485) was mixed and remixed every 15 min up to 3 hours, and then cylinders (10 mm
201 diameter and 50 mm high) were cast. After demolding, slices of 5 mm were cut from the middle of the
202 cylinders and immersed in a sulfate solution. At 28 days, the sample was reduced to ~2 g weight particles and
203 immersed in isopropyl alcohol, and dried at vacuum drier before mercury intrusion the slice. For XRD tests,
204 surface and core samples of the same size were cut from the paste cubes, dried by solvent exchange with
205 acetone, crushed, and the powder was pressed in cylindrical standard sample holders of 16 mm diameter and
206 2.5 mm height. XRD measurements were made using a PANalytical X'Pert PRO MPD Alpha θ/2θ using
207 CuKα_1 radiation working at 45 kV and 40 mA from 4 to 80° 2θ with a step size of 0.017° 2θ and measuring
208 time of 80 seconds.
209

SEM analyses were performed on fracture and cut sections perpendicular to the exposed surfaces of mortars. Fracture sections were dried by solvent exchange with isopropanol, coated with carbon, and examined in a JEOL JSM 6510 microscope at the voltage of 20 kV using secondary and backscattered electrons as well as EDS X-ray analysis. Cut sections were impregnated with epoxy resin, cut, polished, and coated with carbon before determining line profiles using a JEOL JXA-8230 electron microprobe. Energy-dispersive spectrometry (EDS) measurements were conducted using a 20 kV accelerating voltage and 1 nA beam current with a defocused 75 µm spot. The beam was manually placed on characteristic areas with hydrates along a virtual line perpendicular to the external surface at progressive depths up to 7 mm, avoiding air voids, cracks, aggregates, and unreacted clinker particles. This procedure was adopted to minimize data fluctuation due to the heterogeneous microstructure of cement paste in mortar bars and to reach a similar level of the intermixing of phases within the interaction volume. Three-line profiles were measured in each sample with 30 analyzed spots/line and counting times of 60 s for each analyzed point. Standards used for calibration were: wollastonite (Si and Ca), corundum (Al), albite (Na), Fe_2O_3 (Fe), periclase (Mg) and celestine (S). The matrix correction procedure XPP [51] was used to convert specimen X-ray intensity ratios into concentrations. Oxygen was determined by stoichiometry. EDS measurements with analysis totals outside the range 65-85 % were removed after data acquisition based on the thresholds defined by several authors [50-51] for the analysis totals in hydrates.

Scatter plots were prepared to provide insights on the intermixing compounds formed when the penetrating sulfate ions react with the cement-hydrated compounds at different depths in the mortar bars. Based on the line profiles described above, atomic ratios for EDS point analyses were plot on 2D scatter plots. These can be interpreted to assess the composition of the phases present and the intermixing between them. SO_3/CaO ratio is plotted as a function of Al_2O_3/CaO ratio at a different depth from the surface of the C30R, C30O, C15F15R, and C15F15O mortars after 360 days of exposure to the sulfate solution. To discriminate the AFm phases (monosulfoaluminate from the hemicarboaluminate and monocarboaluminate), the (Al/Ca; S/Ca) is used. For these plots, AFt is located at (0.33;0.50), Ms (0.5; 0.33); Mc and Hc (0.5;0), gypsum (0; 1) and C-S-H (0.042; 0.02) [35]. Points are often located along tie-lines between the main cluster points and the theoretical atomic ratio of a corresponding phase. Points not located close to the tie lines are likely to be measurements of more than two phases.

3. RESULTS

3.1. Paste specimens

3.1.1. Mass variation

Figure 1 shows the relative mass variation over time of the paste cubes for each blended cement evaluated immersed in water (Figure 1a) and sulfate solution (Figure 1b). Figure 1c includes images of the cubes exposed to sulfates at different stages of the mass variation test. In both aqueous mediums, all pastes presented a net mass increase throughout the test duration. Mass variation of specimens immersed in the non-aggressive environment reflects the net balance of a combination of processes: mass increase due to water absorption and continued hydration of raw materials and mass reduction caused by leaching of calcium ions [44,52-53]. Figure 1a shows that all cements follow similar trends over time, with an initial stage of rapid mass gain followed by a second stage characterized by a nearly steady plateau. The duration of the first stage varies for each binder composition. For example, the blended cements containing calcined clays develop 70 % of their total relative mass change between the firsts 28-56 days of immersion. On the other hand, the reference composition C30F presents a steadier mass increase, reaching 70 % of its total mass change at nearly 80 days. At the end of the test, the blended cements with ICCR reached the higher relative mass gain (C30R and C15F15R), followed by pastes with ICCO (C30O and C15F15O) and the reference mixture (C30F). These results reflect that compositions with increasing replacement of limestone by calcined clay presumably present lower leaching rates due to the increased calcium demand to form C-S-H gel, which causes a more positive net mass balance.

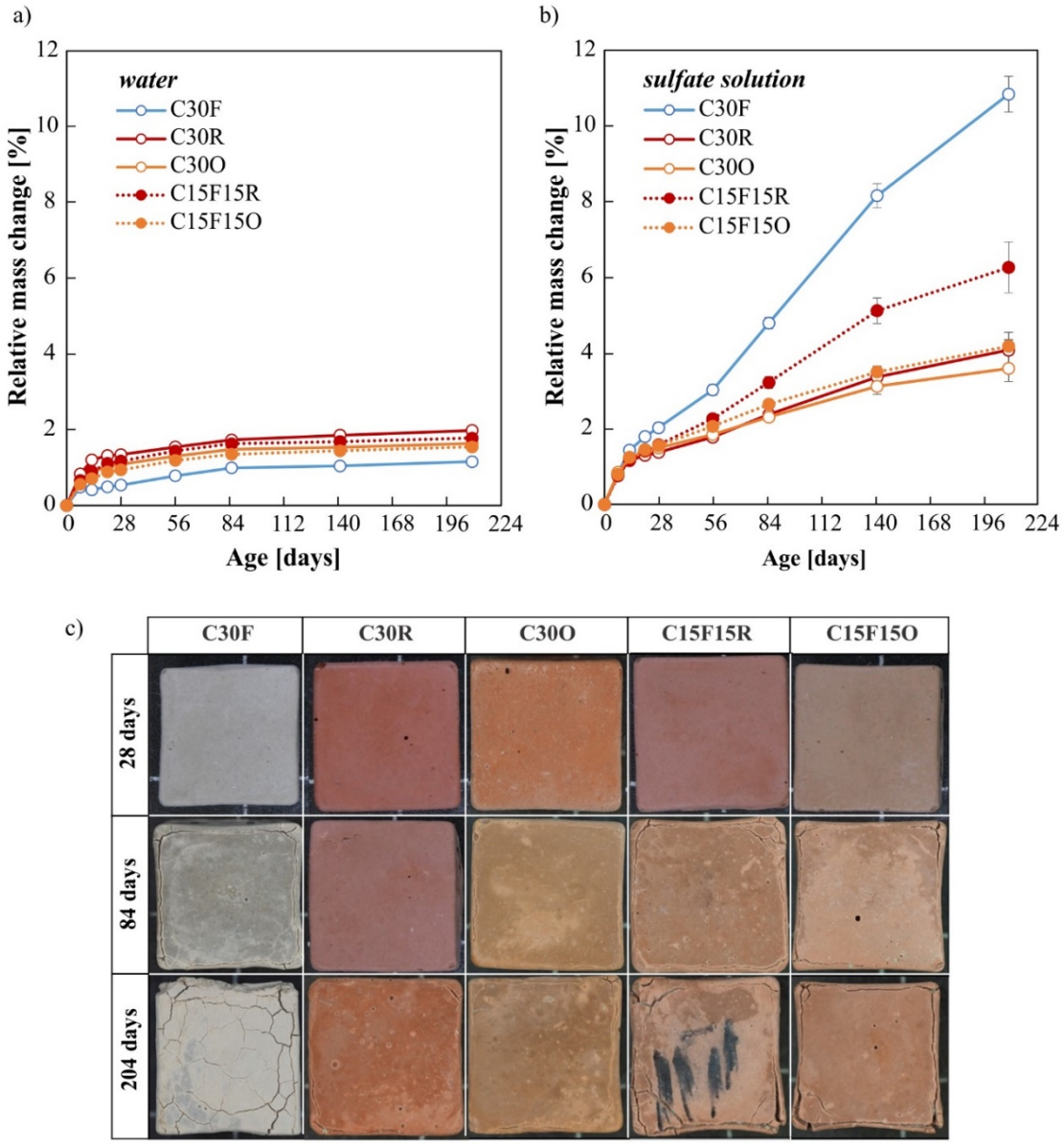

Figure 1. Relative mass variation of pastes cured in: a) water and b) sulfate solution; c) visual appearance of cubes in sulfate solution during the mass variation test.

Figure 1b shows that relative mass changes of specimens exposed to sulfates evolve differently than samples in non-aggressive water, both in terms of trends and magnitude. After a similar first stage, all compositions describe a continuous mass growth until the end of the test. Specimens with increasing calcined clay content show lower relative mass gain rates during the second stage of the attack. In this case, in addition to the combination of processes described above, mass changes depicted in Figure 1b are also defined by sulfate uptake and the formation of secondary products resulting from interactions of the hydrated cement compounds with penetrating sulfate ions [46,54]. Therefore, the additional mass increase measured in all compositions compared to the specimens cured in water is most likely attributed to the formation of secondary sulfate-

containing products and further water absorption due to crack formation during the attack. In this regard, Figure 1c shows that cracking was mainly visible from 90 days along the edges of C30F composition on the typical pattern associated with the ESA. Ternary blends develop cracks near the edges from 90 to 180 days of exposure, while binary calcined clay blends show minor crack formation at the end of the test. The results obtained suggest that even though sulfate attack takes place in all compositions, the use of calcined clay might delay/limit the formation of expansive phases and subsequent damage. The improvement of sulfate resistance seems to be less efficient for lower calcined clay replacement.

The findings derived from measured mass changes are in line with the results presented by Rozière et al. [54]. These authors reported that mixtures with greater CH on hydration might promote the sulfate ion ingress when exposed to sulfate environments due to the higher CH-leaching for these compositions.

3.1.2. Mercury intrusion porosimetry (MIP)

Figure 2 shows the cumulative and volumetric pore size distribution measured on pastes C30F, C30R, and C15F15R immersed in sulfate solution for 28 days. Cumulative intrusion curves include the value of the critical diameter and the threshold pore diameter; no results are reported for mixtures with ICCO, as these were damaged during the execution of the test due to technical problems. Additionally, this figure includes a detail with the relative volume distribution for selected pore ranges to ease the interpretation of the results (<10 nm, 10–50 nm, 50–100 nm, and >100 nm). C30F paste has the highest cumulative pore volume and the critical (65 nm) and threshold radius (140 nm) amongst all compositions evaluated, indicating that the dilution effect of LF replacement generates a large volume of capillary pores that are not reduced later. Results show that the use of ICCR results in a significant reduction of both the total volume of mercury intruded and the critical and threshold pore radius. Increasing ICCR replacement from 15 % to 30 % causes a 60 % reduction of the critical (12 nm) and threshold (30 nm) radius, reflecting the positive pore-refining effect caused by the pozzolanic reaction. The detail included in Figure 2 illustrates that the proportion of pores between 50-100 and above 100 nm is considerably reduced by incorporating calcined clay, whereas the proportion of finer pores increases.

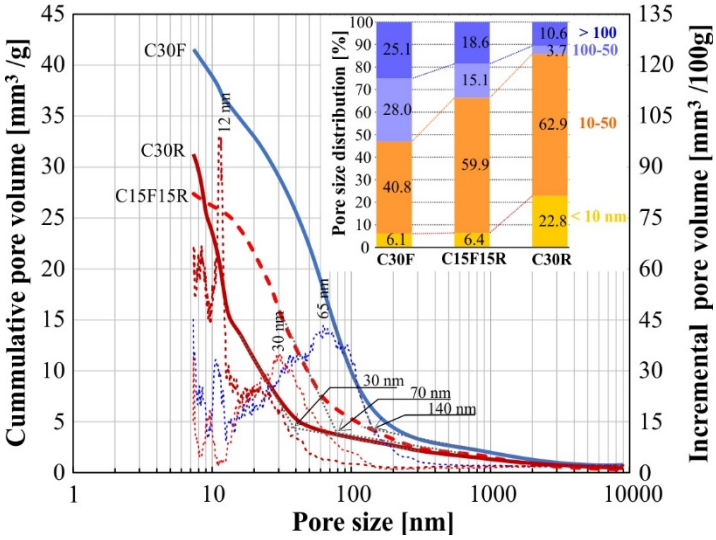

Figure 2: MIP results for pastes exposed 28 days to Na_2SO_4 solution.

3.1.3. Mineralogical composition by X-ray diffraction

Figure 3 shows the XRD patterns obtained from the surface of cubes exposed to sulfate solution for 28 and 204 days. In this figure, the XRD patterns obtained from the corresponding cube stored in water overlap to allow phase comparison between the hydration and the attack. The compounds identified in water curing were CH, ettringite, and the AFm phases as monocarboaluminate (Mc) and hemicarboaluminate hydrated (Hc). In sulfate solution, the hydration/attack compounds found were CH, ettringite, and gypsum. Slight growth of calcite may also occur due to the carbonation. Calcite and quartz come from filler and ICC. Some anhydrous Portland cement phases (especially C_2S) are also detected in both pastes at 28 days.

For C30F in water, Mc (11.67° 2θ) and ettringite (9.08° 2θ) can be detected with low intensity at 28 days. In sulfate solution, ettringite grows considerably compared to the sample in water, while the gypsum formation is incipient. From 28 to 204 days, the highest peak growth is assigned to gypsum (11.59° 2θ), with a consequent decrease in those peaks assigned to CH. Gypsum was confirmed by the presence of a well-defined peak at 20.72° 2θ or a hump before the quartz peak at 20.82° 2θ, and also by the high peak intensity at 29.11°, 31.16°, and 33.34° 2θ. For water curing (Figure 3), the peak at 11.67° 2θ was assigned to monocarboaluminate hydrated, which is confirmed by the clearly defined peak at 23.49° 2θ. The presence of gypsum is discarded by the absence of the hump at the peak at 20.8° 2θ.

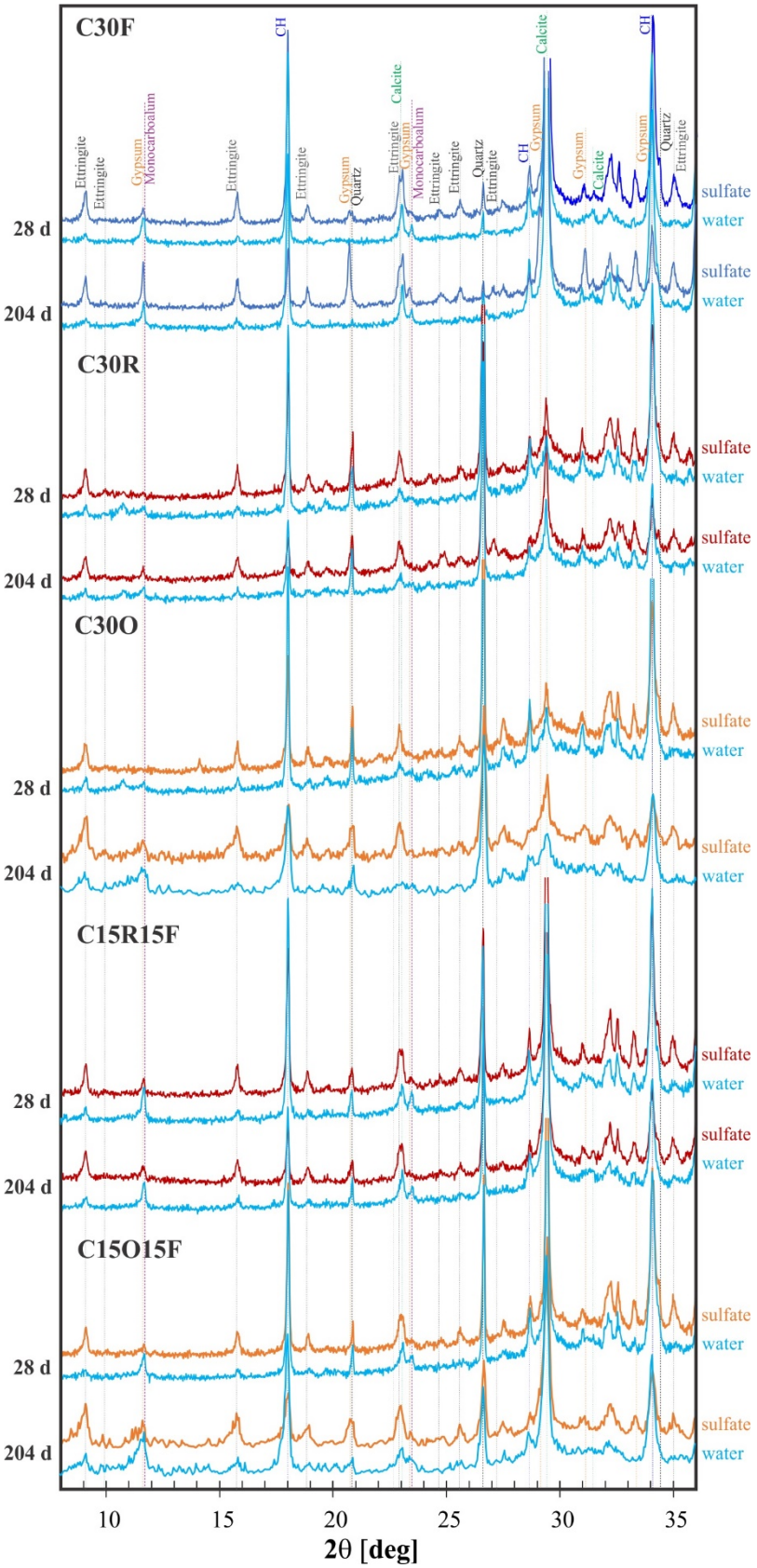

Figure 3. Comparison of XRD pattern of pastes obtained from the surface of cubes exposed to sulfate solution and water for 28 and 204 days.

328 XRD patterns of the C30R and C30O cured in water show the well-defined peaks of ettringite and the poor
329 crystallization of the AFm phase as Hc (10.78° 2θ) and Mc at 28 days. The CH peaks are very intense and
330 remain after 6 months, with the logical reduction due to the pozzolanic reaction. For pastes in sulfate solution,
331 ettringite increases considerably on the surface sample with the consequent decrease in the AFm phases at 28
332 days and a slight reduction in CH. However, gypsum cannot be identified. After 204 days, the peaks
333 corresponding to gypsum experience considerable growth while the intensity of CH peaks is reduced. This CH
334 reduction is attributed to the pozzolanic reaction and the sulfate attack since the CH peaks were lower in the
335 sulfate sample than those measured in the water sample.
336
337 For ternary cements (C15F15R and C15O15F), hydration in water shows intense Mc formation at 28 days,
338 accompanied by stabilization of ettringite [31,56] and CH. At 204 days, the AFt and AFm phases remain
339 stable in the paste, while the pozzolanic reaction reduces the intensity of the CH peaks (18.01° and 34.10° 2θ).
340 For sulfate solution curing, the patterns obtained show an increase of ettringite accompanied by the
341 consumption of the AFm and CH phases from 28 days with respect to curing in water. Gypsum formation
342 appears mildly at 204 days.
343
344 From XRD analysis on the cube surface, it can be concluded that aggressive curing causes ettringite formation
345 from the AFm phases produced during the cement and/or pozzolan hydration and the formation of gypsum at
346 older ages, as established by previous studies [33].
347
348 Figure 4 shows the XRD patterns of samples taken from the core of the paste cubes immersed in sulfate
349 solution at 204 days. Reference patterns of core samples from specimens cured in water are available for
350 C30O and C15O15F mixtures at the same age. C30F patterns obtained reveal that the sulfate ions have
351 reached the core of the cube as both ettringite and gypsum peaks are detected, with similar intensities to those
352 obtained on the surface. These results indicate that the complete volume of the C30F cube is affected by
353 sulfate attack. In mixtures with 30 % ICC replacement (C30R and C30O), even though ettringite peaks are
354 still detected in sulfate curing conditions, their intensity is lower than the obtained in the surface, suggesting a
355 reduced presence of this phase. AFm phases remain stable in the core, and gypsum peaks cannot be assigned
356 in both core samples. Similarly, ternary cements also identify ettringite in the core with a lower peak intensity
357 than the measured on the surface and similar to the reference samples cured in water. The AFm phase is
358 stable, with an Mc-peak intensity greater than the registered in C30R or C30O due to LF presence [56]. CH
359 peaks were found in all samples.
360

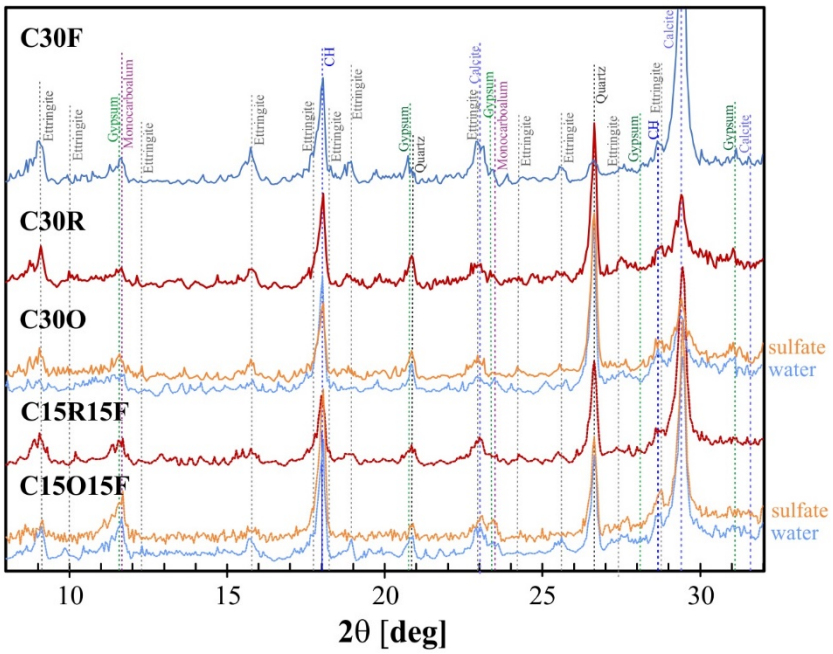

Figure 4. XRD patterns obtained from the core of the cube past exposed to sulfate solution for 204 days.

3.2. Mortar specimens

3.2.1. Length variation

Figure 5 shows the linear expansions of the mortar prisms up to 720 days of sulfate exposure with its corresponding +1/-1 standard deviation bars. Additionally, this figure incorporates horizontal dotted lines to represent the expansion thresholds defined by the ASTM C 1157 at 6 and 12 months to classify blended cement as sulfate resistant (SR). Even though the age of sulfate exposure adopted does not comply with the age prescribed by the standard, the contrast of the expansions obtained with these limits was used qualitatively to compare the sulfate resistance of the different blends evaluated. During the initial exposure up to 28 days, the expansions of the five blended cements present a similar growth, which is likely strongly determined by the swelling associated with water absorption due to the early age of exposure of the specimens (2 days after casting). From then, expansions for mortars with no calcined clay (C30F), binary blended cements with calcined clays (C30R and C30O), and ternary cements (C15F15R and C15F15O) evolve following different trends.

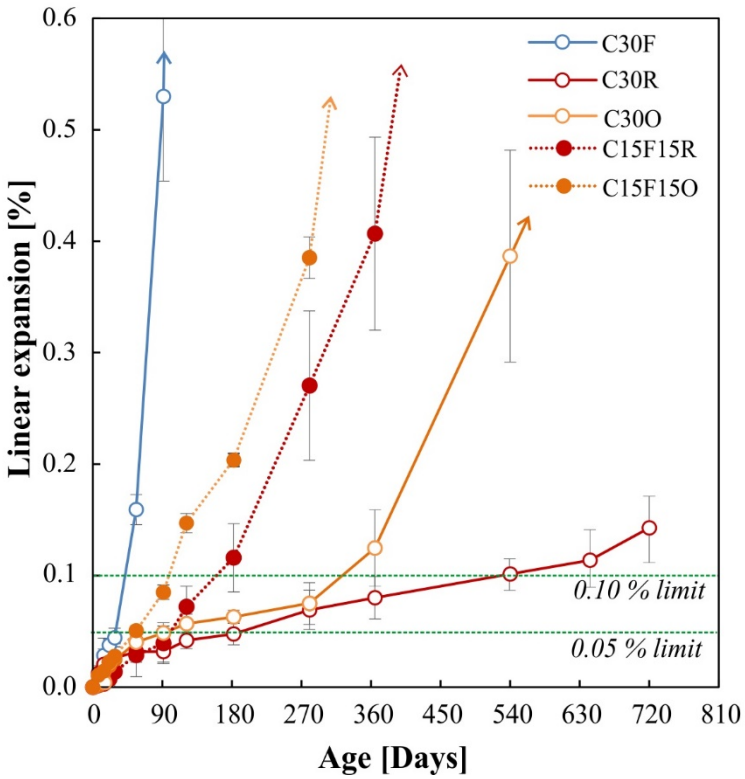

Figure 5. Linear expansion of mortar prisms cured in sulfate solution.

The C30F expansion rate increases exponentially, reaching both 0.05 % and 0.10 % limits defined by the ASTM C 1157 between 28 and 56 days. At 91 days, the mean expansion is higher than 0.50 %, with severe degradation of the specimens, compromising the accuracy of further expansion measurements. On the other hand, C30R and C30O mixtures reduce the average expansion rate from the 8.9 µm/m per day measured between 1-28 days to 1.7 µm/m per day from 28 to 365 days. Mortars with ICCR attain the 0.05 and 0.10 % expansion limit at 192 and 529 days, respectively, and can be classified as SR. However, specimens with ICCO do not comply with the SR requirements since the expansion limit 0.05 % and 0.10 % are reached after 96 and 323 days, respectively. Finally, ternary blends C15F15R and C15F15O show an intermediate behavior between C30F and its corresponding binary blended cements (C30R and C30O), failing both to be qualified as MS and SR. Standard deviation bars reflect the increase over time of the different deterioration levels for the individual specimens, as reported by other authors [41].

The expansion results obtained highlight the positive effects of illitic calcined clays on the sulfate resistance. Since all compositions tested maintained the same initial C_3A content, the better performance of these blended cements cannot be attributed to any dilution effect of the reactivity of the cement. Instead, sulfate resistance is associated with the effects of the pozzolanic reaction on pore size refinement and CH consumption. The CH-consumption during the pozzolanic reaction reduces the availability of CH for ettringite formation. Both positive effects were already identified by other authors, such as [54,55]. However, unlike previous studies,

results reported here have the singularity that mortars were exposed to sulfates shorty after casting, and thus, the kinetics of the pozzolanic reaction have to overcome the kinetics of sulfate attack. Under these circumstances, the results reported here indicate that the pozzolanic reaction progresses faster than sulfate ingress. Thus, calcined clay incorporation can still provide effective pore network refinement and reduce available CH in the bulk mass to limit the transformation of the AFm phase to ettringite.

3.2.2. Mass variation

Figure 6a depicts the relative mass change over time of the mortar prisms during the expansion test. In general, the mass variations obtained for all mortars follow similar trends to the ones described for paste cubes in section 3.1.1. Measurements are characterized by an initial stage of rapid mass gain followed by a second stage where the mass variation increases at a lower rate. The reference composition C30F depicts a minor reduction of mass gain during the second stage, while binary blends with illitic calcined clays present the lower mass gain throughout the test duration. The magnitudes of the relative mass gain in mortar prisms are lower than those obtained for paste cubes, which is attributed to the acceleration effect associated with the lower exposed surface/volume ratio of prisms (1.6 cm^{-1}) compared to cubes (3 cm^{-1}) and the lower degradable cementitious content in the mortars. Since section 3.1.1. already addresses in detail the interpretation of the mass measurements and the results obtained are analogous; the discussion will not be reproduced here.

Figure 6b presents the relationship between length change measurements and relative mass variation. As reported by other authors [52,54], the results obtained show a clear connection between increasing expansions and increasing mass gain for all mortar compositions evaluated. The curves depict an initial segment with a strong mass increase with minor expansions that might correspond to the initial pore filling process with expansive phases and expansion without cracking. Afterward, the mass/expansion relationship is modified, and most compositions undergo a second stage where expansions dominate over mass gain. This stage might reflect the generation of damage and subsequent stiffness reduction of the specimens, leading to rapid expansions. Notice that the composition C30R remained within the first segment throughout the test duration, indicating superior sulfate resistance.

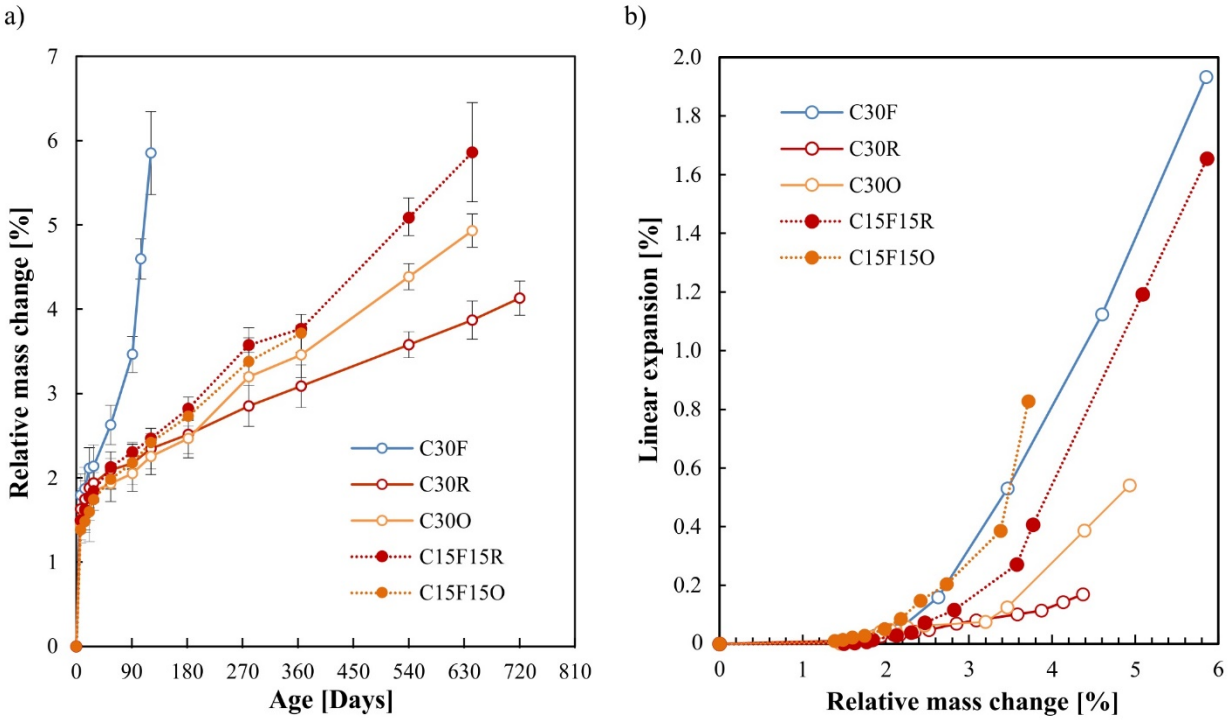

Figure 6. (a) Relative mass variation and (b) Relationship between mass variation and linear expansion of mortar prisms cured in sulfate solution.

3.2.3. Compressive strength

Figure 7 presents the compressive strength obtained on mortar cubes exposed to non-aggressive water (Figure 7a) and sulfate solution (Figure 7b). Additionally, Figure 7c presents the visual aspect of the mortar cubes at 365 days of sulfate exposure. Strength tests were performed at 7, 28, 90, 180, and 365 days on mortars exposed to sulfates and at 28, 90, 180, and 365 days on reference samples. Specimens on non-aggressive water depict usual strength development curves, reaching average strengths between 24.5 - 34.8 MPa at 28 days and 31.1 - 51.3 MPa at 365 days. The C30F exhibits the lowest compressive strength amongst all compositions tested throughout the period evaluated, which is attributed to the negative impact of high levels of limestone addition on the cement paste capillary porosity, as reported by other authors [27,28] and verified by MIP measurements in section 3.1.2. For the same replacement level, mixtures with calcined clay (C30R and C30O) are observed to have higher compressive strength due to the continuous formation of hydrated phases from the pozzolanic reaction [57]. Finally, the ternary blends C15F15R and C15F15O results have an intermediate strength performance.

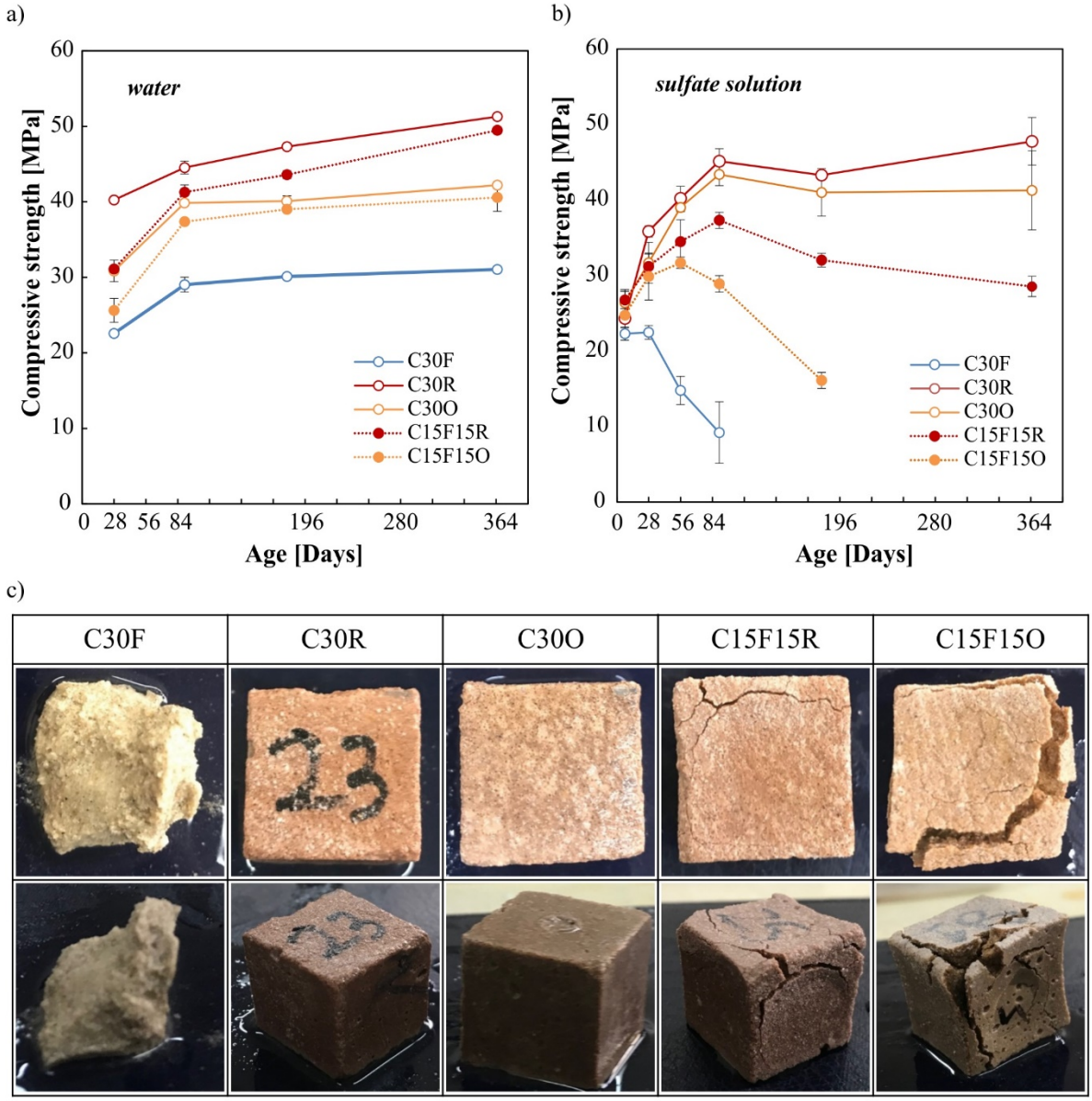

Figure 7. Compressive strength of mortar cubes cured in (a) Water and (b) Sulfate solution. (c) Visual aspect of the samples exposed to sulfates at 365 days: plane view (upper) and axonometric view (down).

In general, measured compressive strengths for specimens exposed to sulfates show similar initial trends to the ones described above for samples cured in non-aggressive water (Figure 7b). However, after an initial period of strength gain, the compressive strength starts to decrease due to cracking and chemical damage caused by the sulfate attack. Both initial strength gain and later strength loss intensities vary significantly for the different compositions tested. C30F presents no strength gain after 7 days of hydration, and the strength drops dramatically from 28 days until 90 days, where samples lose their physical integrity. At 365 days, this blend is entirely disintegrated, as shown in Figure 7c. On the other hand, binary cements with calcined clay addition reach peak strength at 90 days, reflecting the progress of the pozzolanic reaction under aggressive curing and

present null or minor strength loss from this age. In fact, at 90 days, the strengths obtained are greater under aggressive curing than in water, which might be ascribed to the pore filling effect in quantities below the damage onset threshold. Comparing the values obtained at the end of the test between aggressive and non-aggressive curing and the well-preserved mortar surfaces (Figure 7c) suggest negligible deterioration of C30R and C30O from external sulfate attack. As expected, ternary blends C15F15R and C15F15O present intermediate strength evolution between the reference mortar C30F and its corresponding binary blend (C30R or C30O).

3.2.4. Energy-dispersive X-ray spectroscopy (EDS)

Figure 8 shows the penetration profile of SO_3, CaO, and Na_2O for the studied mortars with ICC (C30R, C30O, C15F15R, and C15F15O) at 365 days of sulfate exposure. Penetration profiles for C30F could not be determined due to the total failure experienced by this composition after 1 year of exposure, which reduced the mortar bars to an incoherent mass (as observed in the mortar cubes depicted in Figure 7). Instead, XRD pattern and SEM photographs are presented in the next section to assess the damage caused by the ESA in this particular mortar.

The SO_3 content increases from the external surface to reach a peak concentration within the first few millimeters of mortar. From then, it decreases smoothly until reaching constant concentration. Despite all compositions describing these general trends, differences in the intensity and extent of SO_3 distribution can be observed amongst the different blends examined. Comparison of the moving mean reveals that sulfates penetrate more intensively into the mixtures with ICCO than with ICCR, indicating a superior sulfate resistance of the red illitic calcined clay. For each calcined clay, they are increasing the replacement level from 15 to 30 % results in a reduction of the sulfate penetration. The base content of SO_3 is similar for the different blended cements used. Therefore, the increase in SO_3 must be attributed to the diffusion of ions from the outside. These results agree with the other results reported previously for the mortar specimens (3.2.1, 3.2.2, and 3.2.3).

The CaO-content reflects the effects of leaching on the mortar samples by reducing the CaO concentration near the external surface [58–60]. This phenomenon explains the reduced sulfate content in the solids close to the surface described previously. The extent of the affected region by this phenomenon differs from mixtures with ICCO and ICCR. For the C30R and C15F15R, the leaching affects 1 and 2 mm, respectively whereas, cements mixed with orange clay show a further depth of leaching (3 and 4 mm for C30O and C15F15O, respectively). The CaO-content is higher in both ternary cements. Na_2O profile illustrates a curve with decreasing content from the surface towards the inside of the test cube as a classic diffusion mechanism. The

Na_2O concentration determined in the surface of the C30R is lower than the C15F15R mortar, with a penetration of 2 and 3 mm, respectively. For the ICCO blends, the concentration of Na_2O within the 4 mm from the external surface is significantly higher than the obtained for the ICCR mixtures, as expected from the SO_3 penetration profiles described previously.

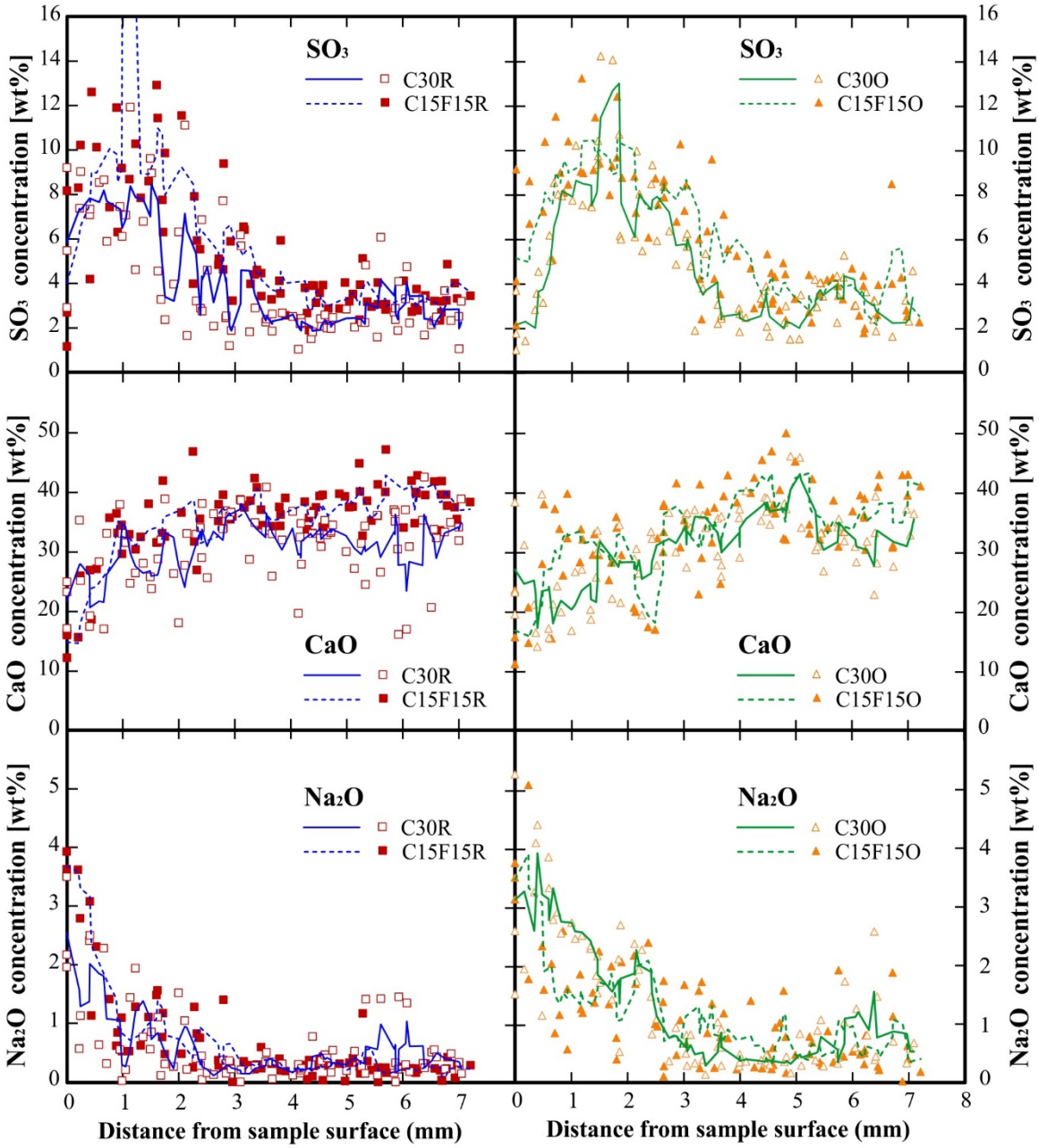

Figure 8: Penetration profile of SO_3, CaO, and Na_2O as function distance from mortar surface at 365 days.

Figure 9 shows the scatter plots of sulfate attack from the external surface towards the interior of the sample, mm to mm, for the different mortars studied. For C30R, EDS analysis points obtained from near the surface (0 to 1 mm) are mainly located near the region corresponding to ettringite-gypsum or on the dashed line between

C-S-H and ettringite intermixed compounds. From 1 to 2 mm depth, the main phases identified are still located within the C-S-H/ettringite intermixed line and few points on the C-S-H/AFm. From 2 - 4 mm, the great majority of phases identified are located on the C-S-H/AFm region, and only a few points indicate a reduced presence of ettringite. Finally, from 4 mm, the main phases identified are monosulfoaluminates from hydration, indicating minor or null effects caused by the ESA.

For the C30O samples, the dots from the surface to 1-mm are distributed on the C-S-H/AFm line. Within this region, no gypsum is identified, which is probably attributed to the increased leaching experienced by this composition at the surface (Figure 8). Between 1 and 2 mm-depth, the main phases identified are ettringite and gypsum. Two well-defined intermixed zones are found from 2 to 4 mm depth: one corresponding to the C-S-H/ettringite line and the other on the C-S-H/AFm line, indicating the ongoing reaction between incoming sulfates and monosulfoaluminate to precipitate ettringite phases. From this depth, the phases identified are mainly located on the C-S-H/AFm intermixed line, with a few points located near the C-S-H/AFt region.

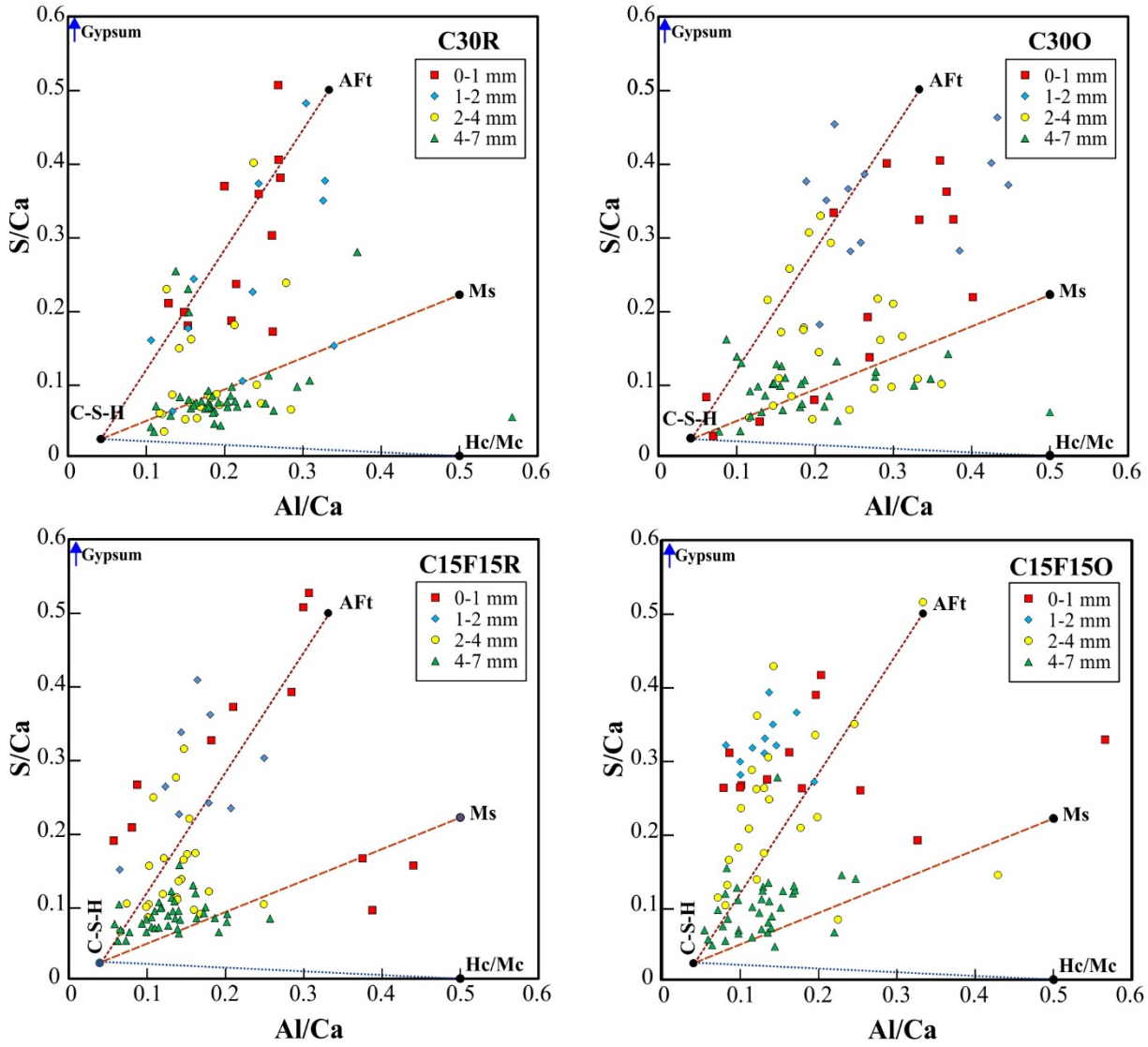

Figure 9: Scatter plots a) C30R; b) C30O; c) C15F15R and d) C15F15O.

The ternary blends analyzed (C15F15R and C15F15O) identify a shift towards the S/Ca axis, indicating an increased presence of gypsum and ettringite at all depths when compared to the binary blends C30R and C30O, respectively. This shift is quite evident on the composition with the ICCO, where almost all monosulfoaluminate from hydration has been transformed into ettringite and gypsum up to 4 mm-depth. Results also reflect a stronger decalcification in the ternary blends. The phases identified in the region from 4 - 7 mm suggest that in the ternary blends, the ESA front is located within this depth, as there is an ongoing reaction between incoming sulfates and monosulfoaluminate to precipitate ettringite phases.

3.2.5. Mineralogical composition of C30F mortars (SEM and X-ray diffraction)

The severe damage developed on the C30F mortars after 365 days of sulfate exposure did not allow the SEM/EDS structured analyses performed on the other mixtures described in section 3.2.4. Instead, the attacked material was sieved, and ground and mineralogical phases were identified based on the XRD pattern. Ettringite and gypsum are the principal compounds formed, and consequently, the calcium hydroxide is practically consumed. Calcite and quartz are also detected from LF and sand. Thaumasite formation cannot be assigned. SEM photographs and EDS analyses shown in Figure 11 confirm the massive presence of ettringite and gypsum on the surface of sand particles, in the bulk paste and growing with radial pattern into the pores.

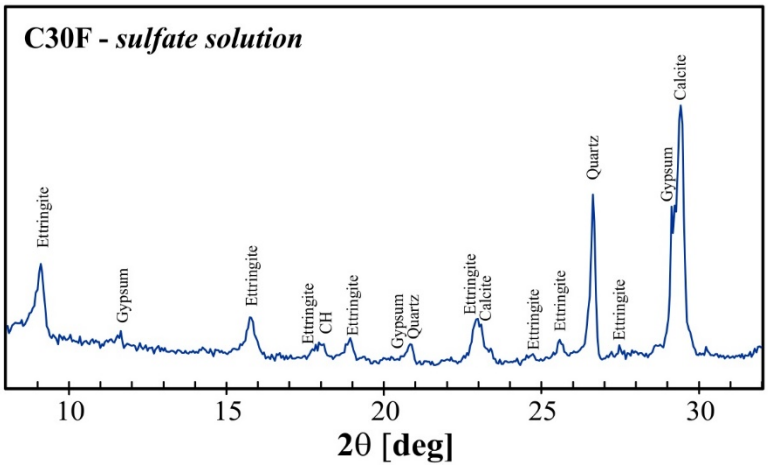

Figure 10: XRD pattern of bulk mass of C30F mortar exposed in sulfate solution at 365 days.

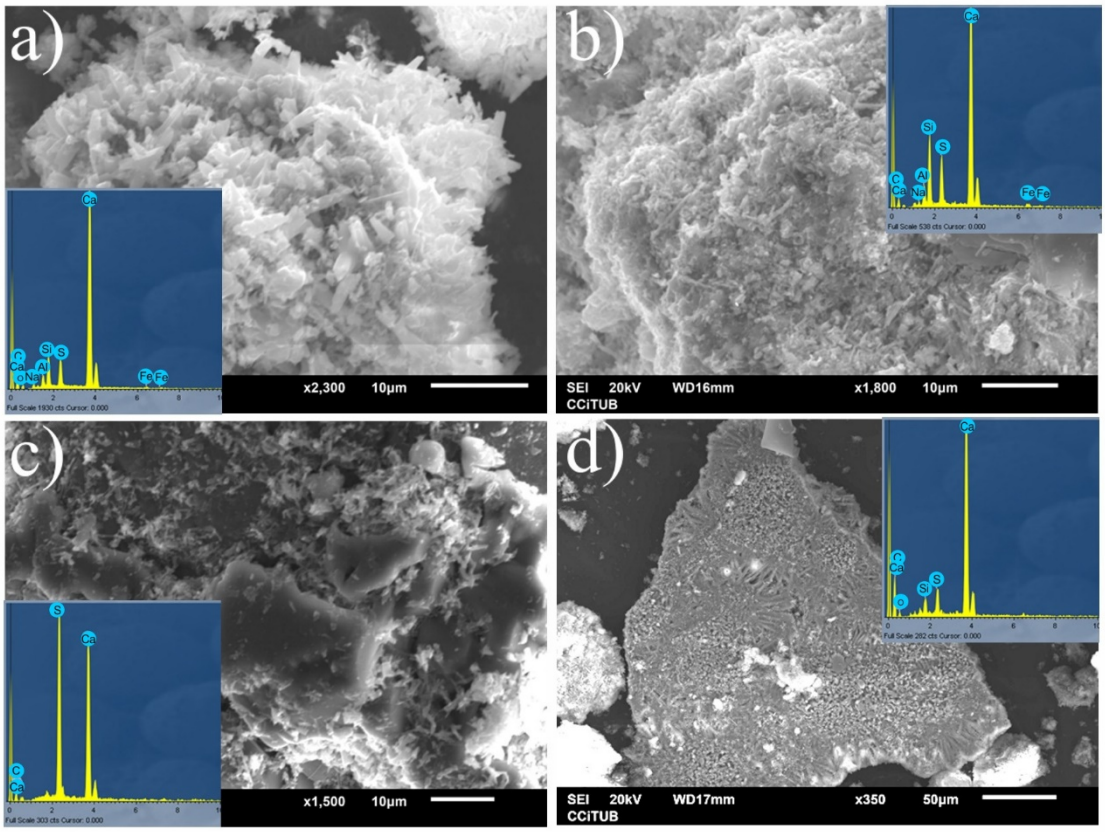

Figure 11: SEM photographs using secondary electron of C30F samples: a) well developed crystals of gypsum and ettringite; b) overall aspect of intermixed crystals of ettringite, gypsum and C-S-H; c) well developed gypsum crystal, and d) arrangement of acicular crystals.

4. DISCUSSION

Mortar bars immersed in the sulfate solution undergo a series of simultaneous chemical and physical transformations triggered by different processes, each of them with different kinetics and extent associated. Immersion of the mortar bars promotes hydration reactions between cementitious and pozzolanic compounds with the water supplied by the solution. At the same time, the external sulfate ions progressively penetrate into the mortar bars and react with the hydration products to form expansive phases within the affected region. Early Ca(OH)2 formed is dissolved and leached out by diffusion, increasing the pH of the solution, which is reestablished periodically by the renewed solution.

The hydration process determines the compounds available to react with the sulfate ions penetrating through the connected porosity, which is determined by the w/cm ratio, the hydration degree, and the dilution effect. The dilution effect depends on the replacement level and the characteristics of the SCM, which can be computed through the effective w/cm in the paste [61]. For C30F, despite the dilution effect is partially

compensated by the stimulation effect caused by the increased number of nucleation points [62], the lack of pozzolanic properties of LF generates a matrix with an effective w/cm ratio of 0.65 with a low or null increase of hydration degree at later ages. This value is too large to obtain effective pore segmentation, which results in a coarse and interconnected porosity (Figure 2) that allows easy paths for sulfate ingress and subsequent ettringite and gypsum formation from the AFm phases and CH (Figure 3) [28]. XRD patterns in water (Figure 3) suggest that AFm phases are mainly present as Mc at 28 days and 6 months. This phase is converted to ettringite when exposed to the sulfate solution, and CH is available. A large proportion of CH was consumed in the paste during the attack (Figure 3), and the consumption was practically completed in mortars (Figure 10), causing a significant deposition of gypsum. Additionally, the coarse porosity of this blend induces a low compressive strength of the material, which weakens the response of the sound inner matrix against the expansive stresses generated during the attack. The combination of low strength and high sulfate penetration results in mass gain (Figures 1b and 6a), surface cracks (Figure 1c), loss of compressive strength (Figure 7b), and rapid expansions (Figure 5).

For binary blended cements with ICCs (C30R and C30O), MIP results shown in Figure 2 indicate that the pozzolanic reaction associated with ICCs hydration effectively refines the pore structure and reduces the paths for sulfate ingress even at the realistic exposure age adopted in this study. In this way, the porous structure of the paste blocking the sulfate ingress into the matrix where they could react with the AFm phases [63]. The design criterium is that the rate of sulfate ingress will be slower than that of the pozzolanic reaction to develop an unconnected pore structure that depends on the space to be filled (dilution effect) and the volume of later hydration products (characteristic of pozzolan). Additionally, XRD patterns at 204 days (Figure 4) confirms CH consumption by the pozzolanic reaction. CH-consumption reduces the availability of Ca^{2+} needed to form the expansive phases, limiting microcracking and new opening of pathways for accelerated sulfate ingress. According to SEM/EDS analyses performed, ICC replacement limits the interactions between sulfate ions and AFm phases to a thin region of a few mm near to the exposed surface during all the periods evaluated. Within this region, AFm and CH is partially transformed to ettringite and gypsum. From this depth, AFm remains unaltered. Such phase distribution is in line with the results presented by Shi et al. [41], obtained from specimens containing MK and calcined montmorillonite exposed to sulfates after 91 days of the previous curing in lime water. The reduced sulfate penetration and expansive phase formation, and higher strength of the matrix are reflected on the macroscale by minor crack formation (Figure 1c and 6c), lower relative mass gain (Figure 1b and Figure 6b), and expansions (Figure 5) and limited or null strength loss (Figure 7). The ICCR displayed the best sulfate resistance amongst the ICCs evaluated, which should be attributed to the increased pozzolanic activity of this calcined clay (see the amorphous content in the Table 1 SAI).

From a chemical point of view, results obtained indicate that CH consumption by the pozzolanic reaction reduces the Ca/Si ratio and contributes, as described by L'Hopital et al. [64], to bind alkalis in the C-A-S-H

system. This phenomenon occurs to re-establish the electrical balance due to the replacement of the Ca^{2+} by the Al^{3+} in the C-A-S-H [65], as reflected in Figure 8 by the increase of alkalis near the surface. Alkalis are presumably bound in the interlayer space of C-A-S-H and show preferred uptake by lower Ca/Si ratios and by high alkali concentrations. As a consequence of alkali uptake, there is a re-arrangement of the C-A-S-H structure. Another critical issue reported by Irbe et al. [66], that uses a high concentration of sulfate, 30 g/L, SO_4^{2-} ions are also bound to other sites in the C-A-S-H. This situation is reflected in the results of the penetration profiles where it can see for SO_3 profile that in the first millimeters, there is an amount of sulfate that may be due to the sulfate reaction and that sulfates binding in the C-A-S-H.

The 15 % ICC replacement adopted in ternary cements (C15F15O and C15F15R) resulted in an increased sulfate resistance compared to the reference C30F mixtures but were not able to prevent the attack as effectively as the 30 % ICC replacement binary blends. Based on the results obtained, 15 % of ICC does not generate enough pozzolanic activity to trigger sufficient pore refinement, CH consumption, and strength gain of the matrix. In addition, the use of 15 % of LF in combination with the ICC increases the effective w/cm ratio (from 0.485 to 0.57) [61], which induces a higher critical pore diameter than the corresponding binary blend with 30 % ICC replacement (Figure 2). As a result, the depth affected by the attack increases, both in terms of expansive phase formation and leaching rate (Figure 8 and 9). These microscale effects are reflected on the macroscale by a higher mass gain and expansion, surface degradation, and strength loss than the 30 % ICC replacement blends.

5. CONCLUSIONS

The following conclusions can be derived from the experimental study presented here:

- Results from mass change, visual inspection, expansion, and compressive strength tests on paste and mortar samples consistently indicate superior sulfate resistance of compositions with high calcined clay content over compositions with limestone filler addition. Since all compositions tested maintained the same initial C_3A content, the better performance of blended illitic cements is associated with the effects of the pozzolanic reaction on pore refinement, strength gain, and CH consumption.
- Microstructure characterization confirms ettringite and gypsum formation after sulfate exposure from the AFm phases and CH produced during the cement and/or pozzolan hydration and reflects the progress of the pozzolanic reaction by CH reduction over time.

- Sulfate profiles obtained by energy-dispersive X-ray spectroscopy show increasing penetration depths with decreasing illitic calcined clay replacement, which confirms the pore refinement effect of calcined clay addition.
- Results show that the physical and chemical changes induced by the pozzolanic reaction effectively reduce the deleterious effects caused by the ESA on realistic exposure conditions (early sulfate exposure). New hydration products are formed, refining the pore network and reducing the penetration of sulfate ions from the external solution. Additionally, the continuous pozzolanic reaction reduces CH availability and thus, the potential reactivity of the AFm phases to form ettringite.

ACKNOWLEDGMENTS

This research was supported by the PIO-004 CIC-CONICET grant awarded by the Comisión de Investigaciones Científicas de la Provincia de Buenos Aires (CICPBA) and the Consejo Nacional de Investigaciones Científicas y Técnicas (CONICET).

REFERENCES

[1] R. Fernandez, F. Martirena, K. Scrivener, The origin of the pozzolanic activity of calcined clay minerals: A comparison between kaolinite, illite and montmorillonite, Cem. Concr. Res. 41 (2011) 113–122. https://doi.org/10.1016/j.cemconres.2010.09.013.

[2] S.A. Miller, V.M. John, S.A. Pacca, A. Horvath, Carbon dioxide reduction potential in the global cement industry by 2050, Cem. Concr. Res. 114 (2018) 115–124. https://doi.org/10.1016/j.cemconres.2017.08.026.

[3] S. Krishnan, A.C. Emmanuel, S. Bishnoi, Hydration and phase assemblage of ternary cements with calcined clay and limestone, Constr. Build. Mater. 222 (2019) 64–72. https://doi.org/10.1016/j.conbuildmat.2019.06.123.

[4] E. Gartner, H. Hirao, A review of alternative approaches to the reduction of CO_2 emissions associated with the manufacture of the binder phase in concrete, Cem. Concr. Res. (2015). https://doi.org/10.1016/j.cemconres.2015.04.012.

[5] Y. Dhandapani, M. Santhanam, Investigation on the microstructure-related characteristics to elucidate performance of composite cement with limestone-calcined clay combination, Cem. Concr. Res. 129 (2020) 105959. https://doi.org/10.1016/j.cemconres.2019.105959.

[6] M. Maier, N. Beuntner, K.-C. Thienel, Mineralogical characterization and reactivity test of common clays suitable as supplementary cementitious material, Appl. Clay Sci. 202 (2021) 105990. https://doi.org/10.1016/j.clay.2021.105990.

[7] S.E. Schulze, J. Rickert, Suitability of natural calcined clays as supplementary cementitious material, Cem. Concr. Compos. 95 (2019) 92–97. https://doi.org/10.1016/j.cemconcomp.2018.07.006.

[8] A. Alujas, R. Fernández, R. Quintana, K.L. Scrivener, F. Martirena, Pozzolanic reactivity of low grade kaolinitic clays: Influence of calcination temperature and impact of calcination products on OPC hydration, Appl. Clay Sci. 108 (2015) 94–101. https://doi.org/10.1016/j.clay.2015.01.028.

[9] A. Tironi, M.A. Trezza, A.N. Scian, E.F. Irassar, Thermal analysis to assess pozzolanic activity of calcined kaolinitic clays, J. Therm. Anal. Calorim. 117 (2014) 547–556. https://doi.org/10.1007/s10973-014-3816-1.

[10] T. Danner, G. Norden, H. Justnes, Characterisation of calcined raw clays suitable as supplementary cementitious materials, Appl. Clay Sci. 162 (2018) 391–402. https://doi.org/10.1016/j.clay.2018.06.030.
[11] K. Scrivener, F. Martirena, S. Bishnoi, S. Maity, Calcined clay limestone cements (LC^3), Cem. Concr. Res. 114 (2018) 49–56. https://doi.org/10.1016/j.cemconres.2017.08.017.
[12] A. Tironi, A.N. Scian, E.F. Irassar, Blended cements with limestone filler and kaolinitic calcined clay: Filler and pozzolanic effects, J. Mater. Civ. Eng. 29 (2017) 04017116. https://doi.org/10.1061/(ASCE)MT.1943-5533.0001965
[13] C. Rodriguez, J.I. Tobon, Influence of calcined clay/limestone, sulfate and clinker proportions on cement performance, Constr. Build. Mater. 251 (2020) 119050. https://doi.org/10.1016/j.conbuildmat.2020.119050.
[14] S. Krishnan, S. Bishnoi, Understanding the hydration of dolomite in cementitious systems with reactive aluminosilicates such as calcined clay, Cem. Concr. Res. 108 (2018) 116–128. https://doi.org/10.1016/j.cemconres.2018.03.010.
[15] Y. Dhandapani, T. Sakthivel, M. Santhanam, R. Gettu, R.G. Pillai, Mechanical properties and durability performance of concretes with Limestone Calcined Clay Cement (LC^3), Cem. Concr. Res. 107 (2018) 136–151. https://doi.org/10.1016/j.cemconres.2018.02.005.
[16] R.G. Pillai, R. Gettu, M. Santhanam, S. Rengaraju, Y. Dhandapani, S. Rathnarajan, A.S. Basavaraj, Service life and life cycle assessment of reinforced concrete systems with limestone calcined clay cement (LC^3), Cem. Concr. Res. 118 (2019) 111–119. https://doi.org/10.1016/j.cemconres.2018.11.019.
[17] D.L. Sparks, Inorganic Soil Components, Environ. Soil Chem. (2003) 43–73. https://doi.org/10.1016/b978-012656446-4/50002-5.
[18] C. He, E. Makovicky, B. Osbæck, B. Øsbæck, Thermal stability and pozzolanic activity of calcined kaolin, Appl. Clay Sci. 9 (1995) 337–354. https://doi.org/10.1016/0169-1317(94)00033-M.
[19] S. Hollanders, R. Adriaens, J. Skibsted, Ö. Cizer, J. Elsen, Pozzolanic reactivity of pure calcined clays, Appl. Clay Sci. 132–133 (2016) 552–560. https://doi.org/10.1016/j.clay.2016.08.003.
[20] G. Habert, N. Choupay, G. Escadeillas, D. Guillaume, J.M. Montel, Clay content of argillites: Influence on cement-based mortars, Appl. Clay Sci. 43 (2009) 322–330.
[21] R. Lemma, E.F. Irassar, V. Rahhal, Calcined illitic clays as portland cement replacements, (2015) 269–276. https://doi.org/10.1007/978-94-017-9939-3.
[22] R.D. Hooton, M.D.A. Thomas, T. Ramlochan, Use of pore solution analysis in design for concrete durability, Adv. Cem. Res. (2010) 203–210. https://doi.org/10.1680/adcr.2010.22.4.203.
[23] C. He, B. Osbæck, E. Makovicky, Pozzolanic reactions of six principal clay minerals: Activation, reactivity assessments and technological effects, Cem. Concr. Res. 25 (1995) 1691–1702. https://doi.org/10.1016/0008-8846(95)00165-4.
[24] G.P. Cordoba, S. V. Zito, R. Sposito, V.F. Rahhal, A. Tironi, C. Thienel, E.F. Irassar, Concretes with calcined clay and calcined shale: Workability, mechanical, and transport properties, J. Mater. Civ. Eng. 32 (2020) 1–11. https://doi.org/10.1061/(ASCE)MT.1943-5533.0003296.
[25] E.F: Irassar, G.P. Cordoba, S. Zito, A. Tironi, V.F. Rahhal, Durability of concrete containing calcined clays: Comparison of illite and low-grade kaolin, in: S. Bishnoi (Ed.), Proc. 3rd Int. Conf. Calcined Clays Sustain. Concr., Elsevier, 2020: pp. 631–640. https://doi.org/10.1007/978-981-15-2806-4_70.
[26] V.L. Bonavetti, C.C. Castellano, E. F. Irassar, Blended cement with illitic calcined clay and calareus material, in: 15th Int. Congr. Chem. Cem., Prague, ID-379, Prague, Czech Republic.
[27] E.F. Irassar, V.L. Bonavetti, M. Gonzalez, Microstructural study of sulfate attack on ordinary and limestone Portland cements at ambient temperature, Cem. Concr. Res. 33 (2003) 31–41. https://doi.org/10.1016/S0008-8846(02)00914-6

[28] T. Schmidt, B. Lothenbach, M. Romer, J. Neuenschwander, K. Scrivener, Physical and microstructural aspects of sulfate attack on ordinary and limestone blended Portland cements, Cem. Concr. Res. 39 (2009) 1111–1121. https://doi.org/10.1016/j.cemconres.2009.08.005.
[29] V. Rahhal, V. Bonavetti, L. Trusilewicz, C. Pedrajas, R. Talero, Role of the filler on Portland cement hydration at early ages, Constr. Build. Mater. 27 (2012) 82–90. https://doi.org/10.1016/j.conbuildmat.2011.07.021.
[30] E.F. Irassar, V.L. Bonavetti, C.C. Castellano, M.A. Trezza, V.F. Rahhal, G. Cordoba, R. Lemma, Calcined illite-chlorite shale as supplementary cementing material: Thermal treatment, grinding, color and pozzolanic activity. Appl. Clay Sci. 179. https://doi.org/10.1016/j.clay.2019.105143
[31] B. Lothenbach, G. Le Saout, E. Gallucci, K. Scrivener, Influence of limestone on the hydration of Portland cements, Cem. Concr. Res. 38 (2008) 848–860. https://doi.org/10.1016/J.CEMCONRES.2008.01.002.
[32] P.C. Aitcin, S. Mindess, Sustainability of Concrete, 2011. https://doi.org/10.1201/9781482266696.
[33] A. Neville, The confused world of sulfate attack on concrete, Cem. Concr. Res. 34 (2004) 1275–1296. https://doi.org/10.1016/j.cemconres.2004.04.004.
[34] M. Collepardi, A state-of-the-art review on delayed ettringite attack on concrete, Cem. Concr. Compos. 25 (2003) 401–407. https://doi.org/10.1016/S0958-9465(02)00080-X.
[35] C. Yu, W. Sun, K. Scrivener, Mechanism of expansion of mortars immersed in sodium sulfate solutions. Cem. Concr. Res. 43, 105–111. https://doi.org/10.1016/j.cemconres.2012.10.001
[36] Ramezanianpour, A.M., Hooton, R.D., Sulfate resistance of Portland-limestone cements in combination with supplementary cementitious materials. Mater. Struct. 46 (2013) 1061–1073. https://doi.org/10.1617/s11527-012-9953-8
[37] E.F. Irassar, M. González, V. Rahhal, Sulphate resistance of Type V cements with limestone filler and natural pozzolana, Cem. Concr. Compos. 22 (2000) 361–368. https://doi.org/10.1016/S0958-9465(00)00019-6.
[38] M. Santhanam, M.D. Cohen, J. Olek, Sulfate attack research - Whither now?, Cem. Concr. Res. 31 (2001) 845–851. https://doi.org/10.1016/S0008-8846(01)00510-5.
[39] Wild, S., Khatib, J.M., O'Farrell, M., Sulphate resistance of mortar, containing ground brick clay calcined at different temperatures. Cem. Concr. Res. 27 (1997) 697–709. https://doi.org/10.1016/S0008-8846(97)00059-8
[40]A. Trümer, H. Ludwig, M. Schellhorn, R. Diedel, Effect of a calcined Westerwald bentonite as supplementary cementitious material on the long-term performance of concrete, Appl. Clay Sci. 168 (2019) 36–42. https://doi.org/10.1016/j.clay.2018.10.015.
[41] E.F. Irassar, G. Cordoba, A. Rossetti, D. Falcone, Sulfate and Alkali-Silica performance of blended cements containing illitic calcined clays, in: Calcined Clays Sustain. Concr. RILEM Bookseries, Vol 16. Springer, 2018: pp. 117–123. https://doi.org/10.1007/978-94-024-1207-9_19.
[42] E.F. Irassar, G. Cordoba, S. Zito, A. Rossetti, V.F. Rahhal, D. Falcone, Durability of blended cements containing illitic calcined clays, 15th Int. Congr. Chem. Cem., Prague, Czech Rep. (2019).
[43] Z. Shi, S. Ferreiro, B. Lothenbach, M.R. Geiker, W. Kunther, J. Kaufmann, D. Herfort, J. Skibsted, Sulfate resistance of calcined clay – Limestone – Portland cements, Cem. Concr. Res. 116 (2019) 238–251. https://doi.org/10.1016/J.CEMCONRES.2018.11.003.
[44] T. Ramlochan, M. Thomas, Effect of metakaolin on external sulfate attack, ACI Symp. Special Publ. 192 (2000) 239–252. https://doi.org/10.14359/5752.
[45] Z. Shi, M.R. Geiker, K. De Weerdt, B. Lothenbach, J. Kaufmann, W. Kunther, S. Ferreiro, D. Herfort, J. Skibsted, Durability of portland cement blends including calcined clay and limestone: Interactions with sulfate, chloride and carbonate ions, RILEM Bookseries. 10 (2015) 133–141. https://doi.org/10.1007/978-94-017-9939-3_17.

[46] T. Ikumi, I. Segura, S.H.P. Cavalaro, Inlfuence of early sulfate exposure on the pore network development of mortars, Constr. Build. Mater. 143 (2017) 33–47. https://doi.org/10.1016/j.conbuildmat.2017.03.081.
[47] N.M. Al-Akhras, Durability of metakaolin concrete to sulfate attack, Cem. Concr. Res. 36 (2006) 1727–1734. https://doi.org/10.1016/j.cemconres.2006.03.026.
[48] E.F. Irassar, A. Tironi, V.L. Bonavetti, M.A. Trezza, C.C. Castellano, V.F. Rahhal, H.A. Donza, A.N. Scian, Thermal treatment and pozzolanic activity of calcined clay and shale, ACI Mater. J. 116 (2019) 133–144. https://doi.org/10.14359/51716717.
[49] E.F. Irassar, V.L. Bonavetti, C.C. Castellano, M.A. Trezza, V.F. Rahhal, G. Cordoba, R. Lemma, Calcined illite-chlorite shale as supplementary cementing material: Thermal treatment, grinding, color and pozzolanic activity, Appl. Clay Sci. 179 (2019). https://doi.org/10.1016/j.clay.2019.105143.
[50] A. Rossetti, T. Ikumi, I. Segura, E. Irassar, Sulfate resistance of blended cements (Limestone-Illite calcined clay) exposed without previous curing, in: S. Bishnoi (Ed.), Proc. 3rd Int. Conf. Calcined Clays Sustain. Concr., Elsevier, 2020: pp. 655–664. https://doi.org/10.23967/dbmc.2020.224.
[51] J.L. Pouchou, F. Pichoir, A simplified version of the "PAP" model for matrix corrections in EPMA. In: D.E. Newbury (ed), Microbeam Anal., (1988) San Francisco Press, pp. 315–318
[52] A.M. Harrisson, N.B. Winter, H.F.W. Taylor, X-ray microanalysis of microporous materials. J Mater Sci Lett 6 (1987) 1339–1340. https://doi.org/10.1007/BF01794611
[53] K.O. Kjellsen, E. Helsing Atlassi, X-ray microanalysis of hydrated cement: Is the analysis total related to porosity?, Cem. Concr. Res, 28(1998) 61-165. https://doi.org/10.1016/S0008-8846(97)00201-9
[54] E. Rozière, A. Loukili, R. El Hachem, F. Grondin, Durability of concrete exposed to leaching and external sulphate attacks, Cem. Concr. Res. 39 (2009) 1188–1198. https://doi.org/10.1016/j.cemconres.2009.07.021.
[55] Z. Shi, S. Ferreiro, B. Lothenbach, M.R. Geiker, W. Kunther, Cement and Concrete Research Sulfate resistance of calcined clay – Limestone – Portland cements, Cem. Concr. Res. 116 (2019) 238–251. https://doi.org/10.1016/j.cemconres.2018.11.003.
[56] V.L. Bonavetti, V.F. Rahhal, E.F. Irassar, Studies on the carboaluminate formation in limestone filler-blended cements, Cem. Concr. Res. 31 (2001) 853–859. https://doi.org/10.1016/S0008-8846(01)00491-4.
[57] G. Marchetti, V. Rahhal, Z. Pavlík, M. Pavlíková, E.F. Irassar, Assessment of packing, flowability, hydration kinetics, and strength of blended cements with illitic calcined shale, Constr. Build. Mater. 254 (2020) 119042. https://doi.org/10.1016/j.conbuildmat.2020.119042.
[58] M.D. Cohen, B. Mather, Sulfate attack on concrete. Research needs, ACI Mater. J. 88 (1991) 62–69. https://doi.org/10.14359/2382.
[59] P.K. Mehta, Mechanism of sulfate attack on portland cement concrete — Another look, Cem. Concr. Res. 13 (1983) 401–406. https://doi.org/10.1016/0008-8846(83)90040-6.
[60] P.W. Brown, An evaluation of the sulfate resistance of cements in a controlled environment, Cem. Concr. Res. 11 (1981) 719–727. https://doi.org/10.1016/0008-8846(81)90030-2.
[61] P. Lawrence, M. Cyr, E. Ringot, Mineral admixtures in mortars: Effect of inert materials on short-term hydration, Cem. Concr. Res. 33 (2003) 1939–1947. https://doi.org/10.1016/S0008-8846(03)00183-2.
[62] E.F. Irassar, Sulfate attack on cementitious materials containing limestone filler - A review, Cem. Concr. Res. 39 (2009) 241–254. https://doi.org/10.1016/j.cemconres.2008.11.007.
[63] J.I. Bhatty, P.C. Taylor, Sulfate Resistance of Concrete Using Blended Cements or Supplementary Cementitious Materials, Portl. Cem. Assoc. (2006).
[64] E.L. Hôpital, B. Lothenbach, K. Scrivener, D.A. Kulik, Alkali uptake in calcium alumina silicate hydrate (C-A-S-H), Cem. Concr. Res. 85 (2016) 122–136. https://doi.org/10.1016/j.cemconres.2016.03.009.
[65] S.Y. Hong, F.P. Glasser, Alkali sorption by C-S-H and C-A-S-H gels: Part II. Role of alumina, Cem. Concr. Res. 32 (2002) 1101–1111. https://doi.org/10.1016/S0008-8846(02)00753-6.

[66] L. Irbe, R.E. Beddoe, D. Heinz, The role of aluminium in C-A-S-H during sulfate attack on concrete, Cem. Concr. Res. 116 (2019) 71–80. https://doi.org/10.1016/j.cemconres.2018.11.012.